Geometry of the charge density wave in the kagome metal math xmlns="http://www.w3.org/1998/Math/MathML">mi>A/mi> msub>mrow>mi mathvariant="normal">V/mi> /mrow>mn>3/mn>/msub>msub>mrow>mi>Sb/mi>/mrow >mn>5/mn>/msub>/math>

H. Miao, H. X. Li, W. R. Meier, A. Huon, H. N. Lee, A. Said, H. C. Lei, B. R. Ortiz, S. D. Wilson, J. X. Yin, M. Z. Hasan, Ziqiang Wang, Hengxin Tan, and Binghai Yan

Phys. Rev. B **104**, 195132 — Published 18 November 2021

DOI: 10.1103/PhysRevB.104.195132

Geometry of the charge density wave in kagomé metal AV_3Sb_5

H. Miao,[1,*] H. X. Li,[1] W. R. Meier,[1] A. Huon,[1] H. N. Lee,[1] A. Said,[2] H. C. Lei,[3] B. R. Ortiz,[4] S. D. Wilson,[4] J. X. Yin,[5] M. Z. Hasan,[5] Ziqiang Wang,[6] Hengxin Tan,[7] and Binghai Yan[7]

[1]*Material Science and Technology Division, Oak Ridge National Laboratory, Oak Ridge, Tennessee 37831, USA*
[2]*Advanced Photon Source, Argonne National Laboratory, Argonne, Illinois 60439, USA*
[3]*Department of Physics and Beijing Key Laboratory of Opto-Electronic Functional Materials and Micro-devices, Renmin University of China, Beijing, China*
[4]*Materials Department and California Nanosystems Institute, University of California Santa Barbara, Santa Barbara, California 93106, USA*
[5]*Laboratory for Topological Quantum Matter and Advanced Spectroscopy (B7), Department of Physics, Princeton, New Jersey 08544, USA*
[6]*Department of Physics, Boston College, Chestnut Hill, Massachusetts 02467, USA*
[7]*Department of Condensed Matter Physics, Weizmann Institute of Science, Rehovot 7610001, Israel*

(Dated: October 12, 2021)

Kagomé lattice is a fertile platform for topological and intertwined electronic excitations. Recently, experimental evidence of an unconventional charge density wave (CDW) is observed in a Z2 kagomé metal AV_3Sb_5 (A= K, Cs, Rb). This observation triggers wide interests on the interplay between frustrated crystal structure and Fermi surface instabilities. Here, we analyze the lattice effect and its impact on CDW in AV_3Sb_5. Based on published experimental data, we show that the 2×2×2 CDW breaks the sixfold rotational symmetry of the crystal due to the phase shift between kagomé layers and can explain the twofold symmetric CDW peak intensity observed by scanning tunneling spectroscopy. The coupling between the lattice and electronic degrees of freedom yields a weak first order structural transition without continuous change of lattice dynamics. Our result emphasizes the fundamental role of lattice geometry in proper understanding of unconventional electronic orders in AV_3Sb_5.

Kagomé lattice is a corner shared triangle network that contains three sites per unit cell [1]. The electronic interference between the three sublattices gives rise to flat band, van Hove singularity (saddle point) and Dirac-fermion in its band structure. It has been predicted that, near the van Hove filling, the combination of high density of state, sublattice interference and non-local Coulomb interaction may yield unconventional Fermi surface instabilities, such as the p-wave charge and spin density waves, d-wave Pomeranchuk instability and f-wave superconductivity [2–7]. Recently, a three-dimensional charge density wave (CDW) that possibly intertwines with superconductivity is observed in a kagomé metal AV_3Sb_5 (A= K, Cs, Rb) [4, 8–20]. While a three-dimensional 2×2×2 superstructure is experimentally identified [14, 18, 21, 22], the nature of the CDW and its interplay with the lattice degree of freedom are under rigorous investigations.

Figures 1a and b show the crystal structure of AV_3Sb_5, which has a space group No. 191 (P6/mmm). The V-Sb slab interlaces with the alkali triangle network along the crystal c-axis. Structurally, there are two Sb positions: Sb1 is located at the center of the V-hexagon and Sb2 is sitting above and below the V-triangles. Density functional theory (DFT) calculations found that the ideal kagomé structure is energetically unstable and favors an inverse star-of-David (ISD) structure at zero temperature [12]. While the ISD distortion of the two-dimensional kagomé lattice preserves the D_{6h} symmetry, recent scanning tunneling spectroscopy (STS) studies found that the CDW superlattice peaks break the sixfold rotational symmetry (Fig. 1d), suggesting a chiral CDW or electronic nematicity [10, 15, 18, 28–30]. Magnetoresistence measurements also found evidence of C_2 symmetry that persists into the superconducting phase [15, 30, 31]. Moreover, as we show in Fig. 1e, unlike well-known CDW materials [23–27, 32–34], CDW in AV_3Sb_5 fails to induce acoustic phonon anomalies near the CDW wavevector, $\mathbf{Q}_{\rm CDW}$, indicating a strong commensurability effect [18]. Here, we explore the CDW by numerically and analytically assessing the structural responses below $T_{\rm CDW}$ in AV_3Sb_5. We show that the three-dimensional ISD structure yields a diffraction pattern that is consistent with x-ray scattering (XRD) and STS measurements [9, 10, 18, 28, 29]. Our analysis supports a CDW in AV_3Sb_5 that preserves the D_{6h} in the kagomé-plane. However, due to the phase shift between kagomé layers, the CDW breaks the sixfold rotational symmetry, C_6, and strongly modifies the CDW superlattice peak intensities. Finally, we show that the coupling between CDW and lattice distortion yields a weak first order phase transition [21, 35] that may be responsible for the absence of acoustic phonon anomaly in AV_3Sb_5 [18].

The diffraction intensity follows, $I(\boldsymbol{Q}) = |F(\boldsymbol{Q})|^2$, where $\mathrm{F}(\boldsymbol{Q})$ is the scattering amplitude. For a crystalline material, $\mathrm{F}(\boldsymbol{Q})$ can be formulated as:

* miaoh@ornl.gov

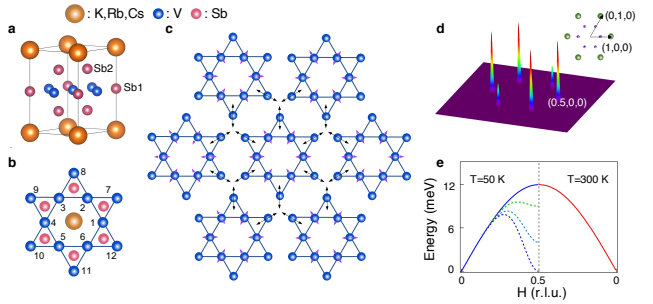

Figure 1. Crystal structure and CDW induced lattice distortion of AV_3Sb_5. (a) and (b) side-view and top-view of AV_3Sb_5 structure. DFT calculations find that the star-of-David (SD) is a local energy minimum at zero temperature, while ISD is the global minimum. (c) shows the SD and ISD lattice distortion of the V-kagomé lattice. Purple and black arrows show atomic distortions of V^{1-6} and V^{7-12} (see (b)), respectively. Distortions of V^{1-6} and V^{7-12} are out-of-phase. The ISD pattern corresponds to V^{1-6}/V^{7-12} moving toward/outward the center of the V-hexagon. (d) reproduces the STS determined CDW peak intensity near Q=0 [10]. The inset shows the Bragg (green) and CDW (purple) peaks in the momentum space. The coordinates are shown in reciprocal lattice units. (e) shows the longitudinal acoustic phonon dispersion at 300 and 50 K [18]. The dashed curves show acoustic phonon anomalies that are expected for strong electron-phonon driven CDW [23–27].

$$F(Q) = \overbrace{\sum_R e^{iQ\cdot R_n}}^{lattice} \overbrace{\sum_j f_j(Q)e^{iQ\cdot r_j}}^{unit\ cell} = \delta_{Q=G} \overbrace{\sum_j f_j(Q)e^{iQ\cdot r_j}}^{unit\ cell} \quad (1)$$

where $\mathbf{R_n}$ and $\mathbf{G}$ are real and reciprocal lattice vectors, respectively. r_j is the j^{th} atomic position in the unit cell. $\mathbf{Q}$ is the total momentum transfer and $f_j(\mathbf{Q})$ is the atomic form factor, which is derived from a Fourier transformation of local density of state (see Appendix A for more details). Below $T_{\rm CDW}$, the formation of CDW distorts the high-temperature structure and gives rise to superlattice peaks at $\mathbf{Q}$=$\mathbf{Q}_{\rm CDW}$.

We first consider the DFT predicted ISD distortions of V-kagomé lattice. Figure 2a schematically shows the ISD distortion, where V^{1-6} and V^{7-12} are breathing out-of-phase with respect to the center of V-hexagon. Figure 2b shows the simulated diffraction pattern of ISD shown in Fig. 2a. The units and directions of the momentum space are shown in Fig. 1d. The scattering region is chosen to match previous XRD measurement at L=0 plane [9, 18], which captures in-plane atomic distortions. Remarkably, we find that ISD reproduces the key feature of the experiment [9, 18], *i.e.*, the CDW peak intensity is significantly larger at $\mathbf{Q}$=(Odd, Int+0.5, 0) or (Int+0.5, Odd, 0), than at $\mathbf{Q}$=($Even$, Int+0.5, 0) or (Int+0.5, $Even$, 0), where $Even$/Odd and Int represent even/odd integers and integers, respectively. As a comparison, we also calculate two more CDW diffraction patterns: (i) the V-stretching shown in Fig. 2c, corresponding to an in-phase breathing of V^{1-6} and V^{7-12} and preserving the D_{6h} symmetry; and (ii) the inversion-symmetry breaking Cs/Sb1 distortion with C_{3h} symmetry as shown Fig. 1e. Apparently, these lattice distortions are incompatible with the empirical selection rules and can be excluded for AV_3Sb_5. To understand the XRD pattern, we calculate the diffraction amplitude of V-kagome lattice:

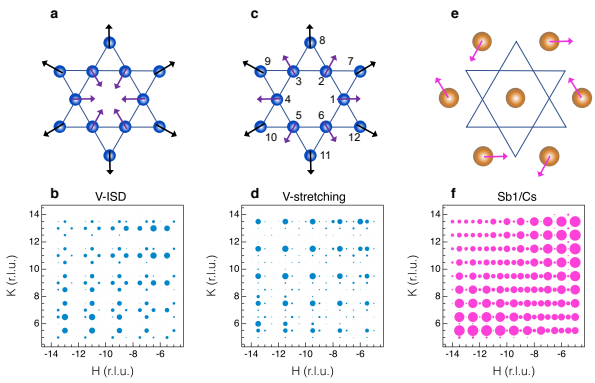

Figure 2. CDW induced lattice distortions in real space and their corresponding diffraction patterns in momentum space. (a) and (b) ISD distortion on V-kagomé sublattice. (c) and (d) V-stretching distortion on V-kagomé sublattice, both of which preserve the D_{6h} symmetry in the kagomé plane. (e) and (f) Sb1/Cs distortion that has C_{3h} symmetry. In the diffraction calculations, the lattice distortions were set to be 1% deviating from the original positions. The units and directions of the momentum space are shown in Fig. 1d. The size of the dots proportional to the intensity of the diffraction pattern.

$$\begin{aligned} F(\mathbf{Q}) = 2\{&cos(\pi H(1+\delta)) + cos(\pi K(1+\delta)) + \\ &cos(\pi(H-K)(1+\delta)) + cos(\pi(H+K)(1+\epsilon)) + \\ &cos(\pi(2H-K)(1+\epsilon)) + cos(\pi(2K-H)(1+\epsilon))\} \end{aligned} \quad (2)$$

where δ and ϵ correspond to V^{1-6} and V^{7-12} distortions, respectively. We assume $|\delta|, |\epsilon| \ll a_0 = 5.4949\mathring{A}$, which are justified by previous XRD measurement, where the CDW superlattice peaks are 3∼5 orders smaller than their nearby fundamental Bragg peaks [18]. Expanding Eq. 2 to the order of $\mathcal{O}(\delta, \epsilon)$:

$$F(\mathbf{Q}) \propto \begin{cases} (H-2K)(\delta+\epsilon) & (even, Int+0.5, 0) \\ H(\delta+3\epsilon) & (odd, Int+0.5, 0) \end{cases} \quad (3)$$

For ISD, ϵ and δ have opposite sign with $(\delta+\epsilon) \sim 0$. Therefore, the CDW superlattice peaks at (even, Int+0.5, 0) are nearly vanishing. We shall note that the star-of-David (SD) distortion [12, 22] also captures the main feature of XRD measurement with subtle differences from ISD structure (see Appendix C). A more

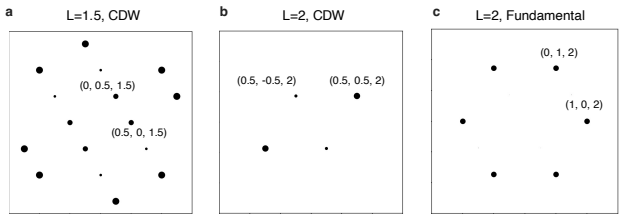

Figure 3. C_2 CDW peak intensity. (a) and (b) show calculated CDW superlattice peak intensity at L=1.5 and 2, respectively. (c) shows the fundamental Bragg peak intensity. The calculation is based on the theoretically refined ISD structure [12]. The size of the dots are proportional to the intensity of the diffraction pattern.

detailed x-ray diffraction measurement and structure refinement are required to distinguish between these two patterns [12].

Since the two-dimensional ISD/SD has the D_{6h} symmetry, the CDW superlattice peaks are expected to show C_6 symmetry. Indeed, based on Eq. 1 and the ISD/SD distortion, we find that:

$$\begin{aligned} &F(0.5,0,0) = F(0,0.5,0) \\ &= F(-0.5,0.5,0) \approx -2\pi(\delta+\epsilon) \end{aligned} \tag{4}$$

The C_6 symmetry of the CDW superlattice peak is, however, incompatible with recent STS studies, where only a C_2 symmetry is observed [10, 18, 28, 29]. As we continue to show below, when CDW is three-dimensional (3D), as reported by recent experimental studies [16, 18, 21, 22, 36], the C_6 symmetry of the CDW peak intensity naturally breaks down to C_2 symmetry. To show the rotational symmetry breaking, we use the theoretically refined 2×2×2 ISD structure of AV_3Sb_5 [12]. Due to the π phase shift between adjacent kagomé layers, the crystal symmetry is lowered from D_{6h} to D_{2h} [7]. Figure 3a and b show the calculated CDW superlattice peak intensity at $L = 1.5$ and $L = 2$, respectively. In agreement with STS studies [16, 18, 21, 22, 36], the CDW superlattice peak intensity only shows C_2 symmetry. In contrast, the fundamental Bragg peak only weakly breaks the C_6 symmetry due to small lattice distortions. We note that in our simulation, the fundamental Bragg peak intensity is three-orders larger than the CDW peak intensity.

Theoretically, three types of CDW order parameters are predicted for AV_3Sb_5, the onsite CDW, bond CDW and imaginary bond CDW involving flux or loop currents [4, 5, 7, 36, 37]. Due to finite electron-phonon coupling, CDW patterns have to respect the point group symmetry of the lattice. For instance, the Sb/Cs1 distortion shown in Fig. 2e is derived from an onsite CDW with C_{3h} symmetry [37]. Our simulations demonstrate that the DFT calculated 2×2×2 superstructure at zero temperature is consistent with experimental observations and therefore support a CDW with D_{6h} symmetry in the kagomé plane. Furthermore, as shown in Fig. 2a-d, the anti-phase breathing of V^{1-6} and V^{7-12} puts another constraint on the CDW pattern in AV_3Sb_5 [37]. Our results, however, do not explain the observed chiral CDW peak intensity in AV_3Sb_5 [10]. Indeed, the chiral CDW keeps the D_{6h} symmetry of the kagomé plane [4] and hence cannot be distinguished by non-resonant x-ray scattering. Instead, the V L-edge resonant x-ray scattering, which selectively enhance electronic excitions from V $3d$-orbital, might be a sensitive probe for this novel electronic order parameter [38].

Finally, we explore how lattice distortion intertwines with the CDW transition. Previous DFT calculations [12] found that the lattice energy is asymmetric with respect to the lattice distortion, η, at zero temperature (Fig. 4). Since CDW always couples with lattice distortions through finite electron-phonon coupling, the asymmetric lattice-distortion energy adds a cubic term in the CDW free energy and leads to a weak first order phase transition. To elaborate it further, we consider an Ising-type Landau free energy on a two-dimensional kagomé lattice:

$$F(T,\psi) - F_0 = A(T)\psi^2 - C\psi^3 + B\psi^4 \tag{5}$$

where $\psi \sim \Delta_{CDW} \sim \eta$. Note the linear term in Eq. 5 can be removed by a linear transformation of ψ. Δ_{CDW} is the CDW gap in single particle spectral function. C is a constant that is proportional to the electron-phonon coupling strength. The hysteresis of the first order phase transition is, $\Delta T = \frac{C^2}{4AB}$. Experimentally, $\Delta T \sim 1$ K [21, 35], suggesting a weak electron phonon coupling in AV_3Sb_5. Indeed, the calculated electron-phonon coupling constant from ref. [12] is in the weak coupling regime and between 0.3-0.46 for AV_3Sb_5, supporting our conclusion. Due to the weak first order phase transition, the change of the lattice dynamics is discontinuous near $T_{\rm CDW}$ and possibly intervenes the softening of the CDW phason mode. Together with the strong commensuratbility effect of the 2×2×2 CDW, the phason gap may remain large above $T_{\rm CDW}$ and failed to yield acoustic phonon softening near the CDW wavevector [18]. It is important to note that the first-order CDW transition is also possible in a pure electronic model without electron-phonon coupling [6, 7]. In this scenario, neither the CDW phason mode nor the acoustic phonon mode soften by cooling towards the $T_{\rm CDW}$.

In summary, we explored the intricate interplay between lattice geometry and CDW in kagomé metal AV_3Sb_5. We prove that the ISD distortion reproduces the XRD and STS measurements. We showed that the coupling between lattice distortions and CDW induces a weak first order transition without continuous phonon softening in AV_3Sb_5.

Acknowledgements: We thank Kun Jiang for stimulating discussion on the interplay between CDW patterns and lattice distortions and Yimian Yang for technical supports. This research was sponsored by the U.S. Department of Energy, Office of Science, Basic Energy Sciences, Materials Sciences and Engineering Division and by the Laboratory Directed Research and Development

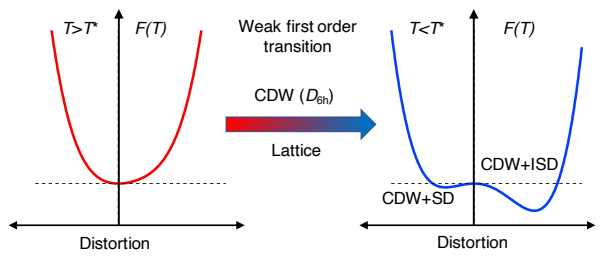

Figure 4. CDW-lattice coupling induced weak first order phase transition. At high temperature, the ideal kagomé lattice is stable and corresponding to the free energy minimum. At zero temperature, ISD is the energy minimum while SD is a local minimum. Near T_{CDW}, the asymmetric lattice free energy adds a cubic term in the CDW free energy through electron-phonon coupling, which, consequently, drive the CDW transition to a weak first order transition.

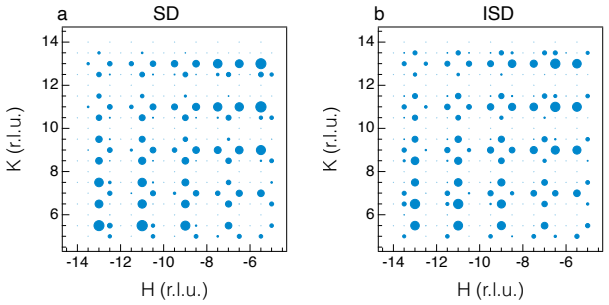

Figure 5. Simulated diffraction intensity. (a) V-SD distortion and (b) V-ISD distortion. In the diffraction calculations, the lattice distortions were set to be 1% deviating from the original positions. The size of the dots are proportional to the intensity of the diffraction pattern.

Program of Oak Ridge National Laboratory, managed by UT-Battelle, LLC, for the U. S. Department of Energy. H.C.L. was supported by National Natural Science Foundation of China (Grant No. 11822412 and 11774423), Ministry of Science and Technology of China (Grant No. 2018YFE0202600 and 2016YFA0300504) and Beijing Natural Science Foundation (Grant No. Z200005). Z.Q.W is supported by the U.S. Department of Energy, Basic Energy Sciences Grant No. DE-FG02-99ER45747. B.Y. acknowledges the financial support by the Willner Family Leadership Institute for the Weizmann Institute of Science, the Benoziyo Endowment Fund for the Advancement of Science, Ruth and Herman Albert Scholars Program for New Scientists, the European Research Council (ERC) under the European Unions Horizon 2020 research and innovation programme (Grant No. 815869) and ISF MAFAT Quantum Science and Technology (2074/19).

Appendix A: Atomic structure factor

The atomic form factor is a Fourier transform of a spatial density distribution of the scattering object. It is defined as:

$$f(\boldsymbol{Q}) = \int \rho(\boldsymbol{r}) e^{i\boldsymbol{Q}\cdot\boldsymbol{r}} d^3\boldsymbol{r} \tag{A1}$$

where $\rho(\boldsymbol{r})$ is the real space electron density. For non-resonant x-ray scattering, the atomic form factor is well approximated by a sum of Gaussians of the form:

$$f(\boldsymbol{Q}) = \sum_{i=1}^{4} a_i exp(-b_i(\frac{\boldsymbol{Q}}{4\pi})^2) + c \tag{A2}$$

The coefficients in Eq. A2 can be found in [39]. When considering the lattice vibrations, the atomic form factor will be modified to:

$$f^{DW}(\boldsymbol{Q}) = f(\boldsymbol{Q}) e^{-\frac{1}{2}\boldsymbol{Q}^2\langle u_Q^2\rangle} \equiv f(\boldsymbol{Q}) e^{-M} \tag{A3}$$

where $\langle u_Q^2\rangle$ is the time averaged mean of squared atomic displacement. In our calculation, Debye-Waller factor has been neglected.

Appendix B: Structural domain

We consider the 2×2×2 superstructure which involves a π-phase shift between the ISD distorted kagomé layers. Assuming the scattering pattern of the two-dimensional ISD structure is $I^{2\times2}(\boldsymbol{Q})$, the scattering intensity of 2×2×2 can be written as:

$$I^{2\times2\times2}(\boldsymbol{Q}) = I^{2\times2}(\boldsymbol{Q}) * |(1 + e^{i\boldsymbol{Q}\cdot\boldsymbol{T}})|^2 \tag{B1}$$

where $\boldsymbol{T}_{a,b,c}$ =(1, 0, 1) or (0, 1, 1) or (1, -1, 1) in the high temperature reciprocal lattice unit. For a measurement in a single structural domain, such as STS, Eq. B2 post strong selection rule. For instance, take $\boldsymbol{T}_a$ =(1, 0, 1), the CDW peak at (0.5, 0, 0) is actually forbidden. For a measurement that covers multiple domains, such x-ray measurement:

$$\begin{aligned} &I^{2\times2\times2}(\boldsymbol{Q}) \\ &= I^{2\times2}(\boldsymbol{Q}) * (|1 + e^{i\boldsymbol{Q}\cdot\boldsymbol{T}_a}|^2 + |1 + e^{i\boldsymbol{Q}\cdot\boldsymbol{T}_b}|^2 + |1 + e^{i\boldsymbol{Q}\cdot\boldsymbol{T}_c}|^2) \\ &\propto I^{2\times2}(\boldsymbol{Q}) \end{aligned} \tag{B2}$$

Therefore, the CDW superlattice peaks determined by multi-domain measurements will be similar to the 2×2 CDW.

Appendix C: Star-of-David distortion

Figure 5 compares diffraction patterns of SD and ISD distortions. While both distortions capture the empirical diffraction selection rules, SD and ISD show subtle differences, for instance, the relative intensity between (H, 13.5, 0) and (H, 12.5 0) are opposite for SD and ISD.

[1] I. Syzi, Statistics of Kagom Lattice, Progress of Theoretical Physics **6**, 306 (1951), https://academic.oup.com/ptp/article-pdf/6/3/306/5239621/6-3-306.pdf.

[2] W.-S. Wang, Z.-Z. Li, Y.-Y. Xiang, and Q.-H. Wang, Competing electronic orders on kagome lattices at van hove filling, Phys. Rev. B **87**, 115135 (2013).

[3] M. L. Kiesel, C. Platt, and R. Thomale, Unconventional fermi surface instabilities in the kagome hubbard model, Phys. Rev. Lett. **110**, 126405 (2013).

[4] X. Feng, K. Jiang, Z. Wang, and J. Hu, Chiral flux phase in the kagome superconductor av_3sb_5 (2021), arXiv:2103.07097 [cond-mat.supr-con].

[5] M. M. Denner, R. Thomale, and T. Neupert, Analysis of charge order in the kagome metal av_3sb_5 (a =k,rb,cs) (2021), arXiv:2103.14045 [cond-mat.str-el].

[6] Y.-P. Lin and R. M. Nandkishore, Complex charge density waves at van hove singularity on hexagonal lattices: Haldane-model phase diagram and potential realization in kagome metals av_3sb_5 (2021), arXiv:2104.02725 [cond-mat.supr-con].

[7] T. Park, M. Ye, and L. Balents, Electronic instabilities of kagome metals: saddle points and landau theory (2021), arXiv:2104.08425 [cond-mat.supr-con].

[8] B. R. Ortiz, L. C. Gomes, J. R. Morey, M. Winiarski, M. Bordelon, J. S. Mangum, I. W. H. Oswald, J. A. Rodriguez-Rivera, J. R. Neilson, S. D. Wilson, E. Ertekin, T. M. McQueen, and E. S. Toberer, New kagome prototype materials: discovery of kv_3sb_5, rbv_3sb_5, and csv_3sb_5, Phys. Rev. Materials **3**, 094407 (2019).

[9] B. R. Ortiz, S. M. L. Teicher, Y. Hu, J. L. Zuo, P. M. Sarte, E. C. Schueller, A. M. M. Abeykoon, M. J. Krogstad, S. Rosenkranz, R. Osborn, R. Seshadri, L. Balents, J. He, and S. D. Wilson, Csv_3sb_5: A $\mathbb{Z}_2$ topological kagome metal with a superconducting ground state, Phys. Rev. Lett. **125**, 247002 (2020).

[10] Y.-X. Jiang, J.-X. Yin, M. M. Denner, N. Shumiya, B. R. Ortiz, G. Xu, Z. Guguchia, J. He, M. S. Hossain, X. Liu, J. Ruff, L. Kautzsch, S. S. Zhang, G. Chang, I. Belopolski, Q. Zhang, T. A. Cochran, D. Multer, M. Litskevich, Z.-J. Cheng, X. P. Yang, Z. Wang, R. Thomale, T. Neupert, S. D. Wilson, and M. Z. Hasan, Unconventional chiral charge order in kagome superconductor KV3Sb5, Nature Materials 10.1038/s41563-021-01034-y (2021).

[11] Q. Yin, Z. Tu, C. Gong, Y. Fu, S. Yan, and H. Lei, Superconductivity and normal-state properties of kagome metal rbv_3sb_5 single crystals, Chinese Physics Letters **38**, 037403 (2021).

[12] H. Tan, Y. Liu, Z. Wang, and B. Yan, Charge density waves and electronic properties of superconducting kagome metals (2021), arXiv:2103.06325 [cond-mat.supr-con].

[13] H. Zhao, H. Li, B. R. Ortiz, S. M. L. Teicher, T. Park, M. Ye, Z. Wang, L. Balents, S. D. Wilson, and I. Zeljkovic, Cascade of correlated electron states in a kagome superconductor csv3sb5 (2021), arXiv:2103.03118 [cond-mat.supr-con].

[14] Z. Liang, X. Hou, W. Ma, F. Zhang, P. Wu, Z. Zhang, F. Yu, J. J. Ying, K. Jiang, L. Shan, Z. Wang, and X. H. Chen, Three-dimensional charge density wave and robust zero-bias conductance peak inside the superconducting vortex core of a kagome superconductor csv_3sb_5 (2021), arXiv:2103.04760 [cond-mat.supr-con].

[15] H. Chen, H. Yang, B. Hu, Z. Zhao, J. Yuan, Y. Xing, G. Qian, Z. Huang, G. Li, Y. Ye, Q. Yin, C. Gong, Z. Tu, H. Lei, S. Ma, H. Zhang, S. Ni, H. Tan, C. Shen, X. Dong, B. Yan, Z. Wang, and H.-J. Gao, Roton pair density wave and unconventional strong-coupling superconductivity in a topological kagome metal (2021), arXiv:2103.09188 [cond-mat.supr-con].

[16] F. H. Yu, T. Wu, Z. Y. Wang, B. Lei, W. Z. Zhuo, J. J. Ying, and X. H. Chen, Concurrence of anomalous hall effect and charge density wave in a superconducting topological kagome metal (2021), arXiv:2102.10987 [cond-mat.str-el].

[17] K. Y. Chen, N. N. Wang, Q. W. Yin, Z. J. Tu, C. S. Gong, J. P. Sun, H. C. Lei, Y. Uwatoko, and J. G. Cheng, Double superconducting dome and triple enhancement of tc in the kagome superconductor csv3sb5 under high pressure (2021), arXiv:2102.09328 [cond-mat.supr-con].

[18] H. X. Li, T. T. Zhang, T. Yilmaz, Y. Y. Pai, C. Marvinney, A. Said, Q. Yin, C. Gong, Z. Tu, E. Vescovo, C. S. Nelson, R. G. Moore, S. Murakami, H. C. Lei, H. N. Lee, B. Lawrie, and H. Miao, Observation of unconventional charge density wave without acoustic phonon anomaly in kagome superconductors av_3sb_5 (a=rb,cs) (2021), arXiv:2103.09769 [cond-mat.supr-con].

[19] X. Zhou, Y. Li, X. Fan, J. Hao, Y. Dai, Z. Wang, Y. Yao, and H.-H. Wen, Origin of the charge density wave in the kagome metal csv_3sb_5 as revealed by optical spectroscopy (2021), arXiv:2104.01015 [cond-mat.supr-con].

[20] Z. X. Wang, Q. Wu, Q. W. Yin, Z. J. Tu, C. S. Gong, T. Lin, Q. M. Liu, L. Y. Shi, S. J. Zhang, D. Wu, H. C. Lei, T. Dong, and N. L. Wang, Unconventional charge density wave and photoinduced lattice symmetry change in kagome metal csv_3sb_5 probed by time-resolved spectroscopy (2021), arXiv:2105.11393 [cond-mat.supr-con].

[21] D.W.Song, L.X.Zheng, F.H.Yu, J.Li, L.P.Nie, M.Shan, D.Zhao, S.J.Li, B.L.Kang, Z.M.Wu, Y.B.Zhou, K.L.Sun, K.Liu, X.G.Luo, Z.Y.Wang, J.J.Ying, X.G.Wan, T.Wu, and X. H. Chen, Orbital ordering and fluctuations in a kagome superconductor csv_3sb_5 (2021), arXiv:2104.09173 [cond-mat.supr-con].

[22] B. R. Ortiz, S. M. L. Teicher, L. Kautzsch, P. M. Sarte, J. P. C. Ruff, R. Seshadri, and S. D. Wilson, Fermi surface mapping and the nature of charge density wave order in the kagome superconductor csv_3sb_5 (2021), arXiv:2104.07230 [cond-mat.supr-con].

[23] C. M. Varma and A. L. Simons, Strong-coupling theory of charge-density-wave transitions, Phys. Rev. Lett. **51**, 138 (1983).

[24] H. Miao, D. Ishikawa, R. Heid, M. Le Tacon, G. Fabbris, D. Meyers, G. D. Gu, A. Q. R. Baron, and M. P. M. Dean, Incommensurate phonon anomaly and the nature of charge density waves in cuprates, Phys. Rev. X **8**, 011008 (2018).

[25] F. Weber, S. Rosenkranz, J.-P. Castellan, R. Osborn, R. Hott, R. Heid, K.-P. Bohnen, T. Egami, A. H. Said, and D. Reznik, Extended phonon collapse and the origin of the charge-density wave in $2h-nbse_2$, Phys. Rev. Lett. **107**, 107403 (2011).

[26] F. Weber, S. Rosenkranz, J.-P. Castellan, R. Osborn, G. Karapetrov, R. Hott, R. Heid, K.-P. Bohnen, and A. Alatas, Electron-phonon coupling and the soft phonon mode in $tise_2$, Phys. Rev. Lett. **107**, 266401 (2011).

[27] A. Kogar, M. S. Rak, S. Vig, A. A. Husain, F. Flicker, Y. I. Joe, L. Venema, G. J. MacDougall, T. C. Chiang, E. Fradkin, J. van Wezel, and P. Abbamonte, Signatures of exciton condensation in a transition metal dichalcogenide, Science **358**, 1314 (2017).

[28] H. Li, H. Zhao, B. R. Ortiz, T. Park, M. Ye, L. Balents, Z. Wang, S. D. Wilson, and I. Zeljkovic, Rotation symmetry breaking in the normal state of a kagome superconductor kv_3sb_5 (2021), arXiv:2104.08209 [cond-mat.supr-con].

[29] N. Shumiya, M. S. Hossain, J.-X. Yin, Y.-X. Jiang, B. R. Ortiz, H. Liu, Y. Shi, Q. Yin, H. Lei, S. S. Zhang, G. Chang, Q. Zhang, T. A. Cochran, D. Multer, M. Litskevich, Z.-J. Cheng, X. P. Yang, Z. Guguchia, S. D. Wilson, and M. Z. Hasan, Tunable chiral charge order in kagome superconductor rbv_3sb_5 (2021), arXiv:2105.00550 [cond-mat.supr-con].

[30] Y. Xiang, Q. Li, Y. Li, W. Xie, H. Yang, Z. Wang, Y. Yao, and H.-H. Wen, Twofold symmetry of c-axis resistivity in topological kagome superconductor csv_3sb_5 with in-plane rotating magnetic field (2021), arXiv:2104.06909 [cond-mat.supr-con].

[31] S. Ni, S. Ma, Y. Zhang, J. Yuan, H. Yang, Z. Lu, N. Wang, J. Sun, Z. Zhao, D. Li, S. Liu, H. Zhang, H. Chen, K. Jin, J. Cheng, L. Yu, F. Zhou, X. Dong, J. Hu, H.-J. Gao, and Z. Zhao, Anisotropic Superconducting Properties of Kagome Metal {CsV}3Sb5, Chinese Physics Letters **38**, 57403 (2021).

[32] T. M. Rice and G. K. Scott, New mechanism for a charge-density-wave instability, Phys. Rev. Lett. **35**, 120 (1975).

[33] M. Hoesch, A. Bosak, D. Chernyshov, H. Berger, and M. Krisch, Giant kohn anomaly and the phase transition in charge density wave $zrte_3$, Phys. Rev. Lett. **102**, 086402 (2009).

[34] G. Grüner, *Density Waves in Solids* (CRC Press, Taylor & Francis Group, Boca Raton, 2018) pp. 1–288.

[35] C. Mu, Q. Yin, Z. Tu, C. Gong, H. Lei, Z. Li, and J. Luo, s-wave superconductivity in kagome metal csv_3sb_5 revealed by $^{121/123}$sb nqr and ^{51}v nmr measurement (2021), arXiv:2104.06698 [cond-mat.supr-con].

[36] N. Ratcliff, L. Hallett, B. R. Ortiz, S. D. Wilson, and J. W. Harter, Coherent phonon spectroscopy and interlayer modulation of charge density wave order in the kagome metals csv_3sb_5 (2021), arXiv:2104.10138 [cond-mat.supr-con].

[37] X. Feng, Y. Zhang, K. Jiang, and J. Hu, Low-energy effective theory and symmetry classification of flux phases on kagome lattice (2021), arXiv:2106.04395 [cond-mat.supr-con].

[38] A. J. Achkar, M. Zwiebler, C. Mcmahon, F. He, R. Sutarto, I. Djianto, Z. Hao, G. D. Gu, A. Revcolevschi, H. Zhang, Y. Kim, J. Geck, and D. G. Hawthorn, Nematicity in stripe ordered cuprates probed via resonant x-ray scattering, Science **351**, 1 (2016).

[39] P. J. Brown, A. G. Fox, E. N. Maslen, M. A. O'Keefe, and B. T. M. Willis, Intensity of diffracted intensities, International Tables for Crystallography **C**, 554 (2006).